



Biased activation of the receptor tyrosine kinase HER2

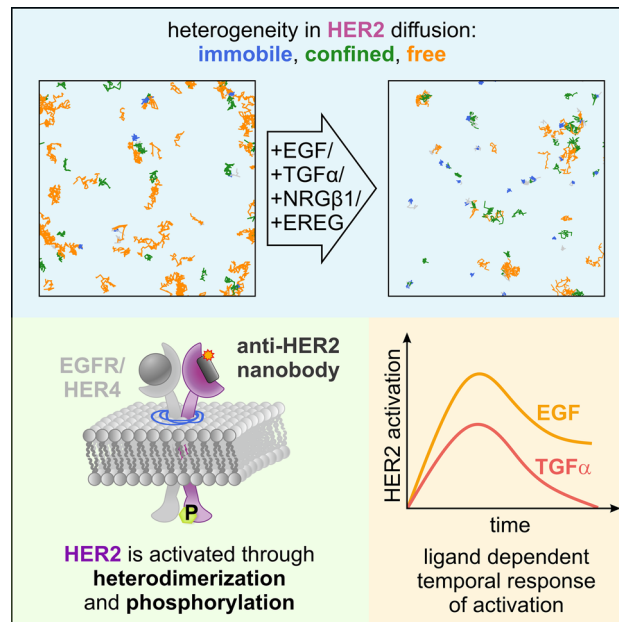
Claudia Catapano¹ · Johanna V. Rahm¹ · Marjan Omer^{2,3} · Laura Teodori^{2,3} · Jørgen Kjems^{2,3} · Marina S. Dietz¹ · Mike Heilemann¹

Received: 22 December 2022 / Revised: 20 April 2023 / Accepted: 11 May 2023 / Published online: 20 May 2023
© The Author(s) 2023

Abstract

HER2 belongs to the ErbB sub-family of receptor tyrosine kinases and regulates cellular proliferation and growth. Different from other ErbB receptors, HER2 has no known ligand. Activation occurs through heterodimerization with other ErbB receptors and their cognate ligands. This suggests several possible activation paths of HER2 with ligand-specific, differential response, which has so far remained unexplored. Using single-molecule tracking and the diffusion profile of HER2 as a proxy for activity, we measured the activation strength and temporal profile in live cells. We found that HER2 is strongly activated by EGFR-targeting ligands EGF and TGF α , yet with a distinguishable temporal fingerprint. The HER4-targeting ligands EREG and NRG β 1 showed weaker activation of HER2, a preference for EREG, and a delayed response to NRG β 1. Our results indicate a selective ligand response of HER2 that may serve as a regulatory element. Our experimental approach is easily transferable to other membrane receptors targeted by multiple ligands.

Graphical abstract



Keywords HER2 · Receptor tyrosine kinase · Live-cell imaging · Single-particle tracking · Biased signaling

Introduction

Receptor tyrosine kinases (RTKs) play a pivotal role in a multitude of fundamental processes such as proliferation, differentiation, and migration [3]. They are classified into numerous subfamilies based on functional or structural similarities, where each receptor group binds characteristic growth factors [53, 54]. Growth factor binding to receptors initiates cellular signal transduction by inducing RTK dimerization, tyrosine phosphorylation, and recruitment of downstream signaling proteins [3, 12].

One of the best-studied subfamilies of receptor tyrosine kinases is the ErbB family with its four receptors HER1-4 and a wide range of related growth factors [47]. All four receptors HER1-4 are structurally related to the epidermal growth factor receptor (EGFR/ErbB1/HER1), which was identified first in 1975 [2]. The discovery of HER2 [9], HER3 [29], and HER4 [40] followed in subsequent years. The ErbB receptor family is involved in a variety of biological activities such as cell differentiation, cell migration, and organ development [4, 15, 39]. Mutations in these proteins may lead to dysfunctions resulting in various diseases, such as cancer and inflammation. This renders the ErbB family a prominent therapeutic target [10, 50].

EGFR, HER3, and HER4 bind in total 11 known cognate ligands. A first group of ligands, comprising amphiregulin, epidermal growth factor (EGF), epigen, and transforming growth factor α (TGF α), exclusively binds to and activates EGFR. The second group of ligands, comprising betacellulin, epiregulin (EREG), and the ectodomain shredded heparin-binding EGF-like growth factor, bind EGFR as well as HER4. The third group are the neuregulins (NRG) 1–4, which all bind HER4, and NRG1 and NRG2 also bind to HER3 [32]. HER2 is an orphan receptor, without any known ligand. Activation occurs through the formation of heterodimers with the other three receptors from this sub-family [18], which is likely facilitated by the extracellular domain of HER2 adopting a conformation similar to that of ligand-bound EGFR, HER3, or HER4 [7]. EGF and TGF α strongly bind to and activate EGFR, leading to EGFR homodimerization [47] and also the formation of EGFR/HER2 heterodimers [32]. EREG binds to HER4 and EGFR, and the formation of heterodimeric complexes with HER2 was reported [53]. NRG β 1 binds to both HER4 and HER3 [5, 25]. It is interesting to note that these four receptors orchestrate many different cellular functions and that this might be regulated by their ligands displaying different receptor-binding specificities and affinities, and a different propensity to engage into heterodimers [51].

Single-particle tracking (SPT) is a powerful method to investigate the mobility of membrane proteins and

to associate this information with the activation states of receptors [24, 33, 36]. For example, a recent study revealed that the receptor tyrosine kinase VEGFR-2 shows diverse modes of activation following the binding of its cognate ligand VEGF [44].

Here, we used SPT to measure the diffusion of single HER2 receptors in the plasma membrane of living cells in resting and ligand-stimulated conditions. We extracted the diffusion coefficient and mode, and from that inferred the activation of HER2 through heterodimerization with ligand-binding receptors. We observed that the global diffusion coefficient of HER2 decreases in ligand-treated cells. Analysis of the diffusion modes revealed that the fraction of immobile receptors increased at the expense of the freely diffusing population. For EGFR-binding ligands, we observed a stronger activation of HER2 in cells treated with EGF, compared to cells treated with TGF α . Also, we found a stronger activation of HER2 in cells treated with EREG, targeting HER4 and EGFR, as compared to NRG β 1, targeting HER3 and HER4. We further refined the experimental protocol and followed the diffusion coefficient and the different diffusion modes over time for a total of 25 min by measuring multiple cells sequentially. We show that the population of immobile receptors over time correlates with the phosphorylation level of HER2, which was determined at different time points using western blotting. From the time-resolved SPT data, we obtained a temporal profile of HER2 activation in live cells that showed specific features in activation strength, time of maximum activation, and desensitization profile for each ligand.

Materials and methods

Cell culture

HeLa cells (German Collection of Microorganisms and Cell Cultures GmbH, Braunschweig, Germany) were cultured in growth medium (GM), consisting of high glucose Dulbecco's modified Eagle medium (DMEM) with 1% GlutaMAX, 10% fetal bovine serum (FBS), 100 U/mL penicillin, and 100 μ g/mL streptomycin (all from Gibco Life Technologies, Waltham, MA, USA), at 37 °C and 5% CO₂ in an automatic CO₂ incubator (Model C150, Binder GmbH, Tuttlingen, Germany). For SPT experiments, round coverglasses (25 mm diameter, 0.17 mm thickness, VWR International, Radnor, PA, USA) were passivated and functionalized with PLL-PEG-RGD [20] and inserted into six-well plates (Greiner Bio-One, Kremsmünster, Austria) [20]. Cells were seeded to a density of 5×10^4 cells/well for SPT experiments with HER2 and 20×10^4 cells/well for SPT experiments with TMD and GPI and grown at 37 °C and in 5% CO₂ for 3 days.

Nanobody expression and purification

The HER2-specific nanobody, 2Rs15d [55], was expressed in *E. coli* with a C-terminal click handle for site-specific conjugation, as previously described [52]. In brief, WK6 *E. coli* cells were co-transformed with a suppressor plasmid, pUltra, and an expression plasmid, pMECS, encoding the nanobody sequence (Supplemental Note 1) with an N-terminal pelB leader sequence, a C-terminal hexahistidine tag (6xHis), and an amber stop codon (TAG) positioned on the C-terminal right before the 6xHis-tag. A discrete colony was grown at 37 °C, 220 rpm until optical density (OD₆₀₀) reached between 0.8 and 0.9. At this OD, the unnatural amino acid, 4-azido-L-phenylalanine (1 mM or 0.202 g/L), was added to the culture following induction with IPTG (1 mM) and grown at 18 °C and 200 rpm for a total of 16 h. The next day, cells were harvested and the nanobodies extracted by periplasmic extraction following affinity chromatography purification using the Ni-NTA column on an Äkta Start System (Cytiva, Marlborough, MA, USA). The purity of the nanobodies was verified by SDS-PAGE gel and Urea PAGE gel.

Nanobody labeling

The azide-modified 2Rs15d nanobody was reacted with a 2.5-fold molar excess Cy3B-PEG6-DBCO in 1 × PBS in a total volume of 100 µL at 21 °C and 600 rpm for 16 h. SDS-PAGE gel evaluation of the reaction showed a 100% labeling of the nanobody. Excess dye was removed using a PD MiniTrap G-10 gravity column (Cytiva) following the manufacturer's recommendations. The Cy3B-labeled nanobody was eluted in a total volume of 0.5 mL 1 × PBS. The purity of the eluted fractions was assessed by SDS-PAGE prior to use for further experiments.

Sample preparation

Coverglasses were mounted into custom-built holders and rinsed once with 600 µL 1 × Live Cell Imaging Solution (LCIS) (Invitrogen, Waltham, MA, USA). 600 µL pre-warmed LCIS was added to holders and cooled to room temperature over 15 min. HER2 was labeled with Cy3B-labeled nanobody (2Rs15d) [52] at a concentration of 2 nM and 10 min prior to the measurements.

For stimulated cells, 20 nM epidermal growth factor (EGF) (#AF-100-15), transforming growth factor alpha (TGFα) (#100-16A), neuregulin beta 1 (NRGβ1) (#100-03), or epiregulin (EREG) (#100-04) (all from PeproTech, Waltham, MA, USA) were added 5 min after measurement start. SPT experiments were conducted between 21 and 23 °C (Fig. S9).

As negative controls, an artificial transmembrane protein (TMD) fused to monomeric enhanced green fluorescent

protein (mEGFP) [56] and a fusion construct of mEos3.2 and glycosylphosphatidylinositol (GPI)-anchor signal peptide of the human folate receptor (Harwardt et al. 2018) was used. The pSems-mEGFP-TMD plasmid was kindly provided by the group of Jacob Piehler (University of Osnabrück, Germany). 100 ng/well pSems-mEGFP-TMD plasmid and 2.25 µg/well sheared salmon sperm DNA (#AM9680, Invitrogen) or 500 ng/well of the pN1-GPI-mEos3.2 plasmid and 1.5 µg/well sheared salmon sperm DNA were transfected using Lipofectamin 3000 (Thermo Fisher Scientific) following the manufacturer's protocol in six-well plates. Transfected cells were incubated overnight at 37 °C and 5% CO₂. Prior to microscopy experiments, cells were washed with 600 µL prewarmed LCIS, 600 µL fresh LCIS was added, and the solution incubated for 15 min at room temperature. The mEGFP-TMD was eventually labeled with 0.5 nM of the mEGFP-targeting FluoTag[®]-Q nanobody labeled with AbberiorStar635P (NanoTag Biotechnologies, Göttingen, Germany) next to EGF addition for the ligand-stimulated condition 5 min prior to measurements. For pN1-GPI-mEos3.2, the fluorescent protein mEos3.2 was tracked, and EGF was added for the ligand-stimulated condition 5 min prior to measurements.

Single-molecule microscopy

Data were acquired on a commercial widefield microscope (N-STORM; Nikon, Düsseldorf, Germany) equipped with an oil-immersion objective (100× Apo TIRF oil; NA 1.49), operated in total internal reflection fluorescence (TIRF) mode, and a 1.5× magnification lens was inserted into the detection beam path for measurements of HER2 and GPI. As excitation light source for Cy3B and mEos3.2, a laser emitting at 561 nm was used and operated at an irradiation intensity of 6.3 W/cm² or 30 W/cm², respectively. The fluorescent protein mEos3.2 was photoconverted to its orange fluorescent state using a 405 nm laser with the intensity adapted to the expression level in single cells. AbberiorStar635P was excited with a laser emitting at 647 nm at 0.6 kW/cm². Fluorescence emission was detected with an electron-multiplying charge-coupled device (EMCCD; Andor iXon, DU-897U-CS0-BV; Andor, Belfast, UK) using an EM gain of 300 (for Cy3B) or 200 (for AbberiorStar635P and mEos3.2), a pre-amplifier gain of 3 and a read-out rate of 17 MHz with activated frame transfer. Images of 256 × 256 pixels were acquired with 157 nm pixel size for experiments with TMD and 105 nm pixel size for experiments with HER2 and GPI.

The microscope was controlled by *NIS Elements* (v4.30.02, Nikon) and *µManager* (v1.4.22) [14]. For each cell, a total of 1000 frames was recorded at an integration time of 20 ms. To record a time series, 25 cells were imaged sequentially during an acquisition time of about 30 min.

To record time series for cells that were stimulated with a ligand, the ligand was added after five cells were measured.

Data analysis

Single emitters were localized with *ThunderSTORM* (version dev-2016-09-10-b1 [38], a plugin for *Fiji* [46]). Parameters for the tracking analysis (*precision*, *exp_noise_rate*, *diffraction_limit*, *exp_displacement*, and *p_bleach*) were determined from localization data following a previously published procedure using *SPTAnalyser* [41, 42]. The *exp_noise_rate* and *precision* were calculated individually per cell, whereas the parameters *diffraction_limit* (HER2: 17 nm, TMD: 23 nm, GPI: 30 nm), *exp_displacement* (HER2: 117 nm, 82 nm, TMD: GPI: 165), and *p_bleach* (HER2: 0.064, TMD: 0.0138, GPI: 0.095) were averaged and used globally for all cells. The switching probability was set to 0.01. Localizations were connected to trajectories using the software package *swift* (v0.4.2) (Endesfelder et al., manuscript in prep.) with the aforementioned parameters. MSD analysis (fitting length of 4 data points for calculation of diffusion coefficients), filtering (minimal trajectory length of 20), and assignment of diffusion types were performed in *SPTAnalyser* [41]. Segments were classified as immobile with a threshold of a minimal diffusion coefficient D_{\min} (HER2) = 0.0084 $\mu\text{m}^2/\text{s}$, D_{\min} (TMD) = 0.0037 $\mu\text{m}^2/\text{s}$, D_{\min} (GPI) = 0.0086 $\mu\text{m}^2/\text{s}$ calculated from the third quartile of the dynamic localization precision [35, 45]. Diffusion coefficients and modes were calculated per individual cell and averaged over all cells. For comparison of global values for diffusion coefficients and fractions of diffusion types, the data recorded for cells from time intervals of 0–20 min were grouped. To correct for fluctuations between the resting condition in different measurements, the relative occurrence of diffusion modes in the first 5 min of measurements (–5 min interval, prior to ligand addition) were aligned (uncorrected data are shown in Fig. S6). Time course analyses were performed by grouping diffusion coefficients and modes in time groups of 1 or 5 min to minimize the contribution of cell heterogeneity [44].

Swift version 0.4.2, used in this manuscript, and all subsequent versions of the *swift* software, as well as documentation and test data sets, can be obtained on the *swift* beta-testing repository (<http://bit.ly/swiftracking>). The home-written software *SPTAnalyser* in Python (3.7.6) estimates parameters for tracking with *swift* and executes diffusion state analysis and transition counting. *SPTAnalyser* has a graphical user interface with adaptable analysis parameters and assists in processing large amounts of data by creating macros for *ThunderSTORM* and batch files for *swift*. *SPTAnalyser* is also compatible with *PALMTracer* (Bordeaux Imaging Center), which is a software for localization and tracking available as a plugin for *MetaMorph* (Molecular

Devices, Sunnyvale, CA, USA). The source code of *SPTAnalyser*, together with a detailed manual, is available from <https://github.com/JohannaRahm/SPTAnalyser>.

Western blotting

0.9×10^6 HeLa cells were seeded onto 10 cm cell culture dishes (Greiner Bio-One, Kremsmünster, Austria) in GM and grown at 37 °C and 5% CO₂. In the evening of the 3rd day, cells were starved with serum-free GM overnight. Cells were stimulated with 20 nM of one of the respective ligands EGF, TGF α , NRG β 1, or EREG in serum-free GM and incubated for 2, 5, or 30 min. For the control western blot (Fig. S1), cells were incubated with 20 nM EGF and 2 nM nanobody for 5 min. Afterward, cells were rinsed with ice-cold 1 \times Dulbecco's phosphate-buffered saline (PBS), pH 7.4 (Gibco Life Technologies, #14040133), and incubated for at least 2 min on ice prior to adding lysis buffer consisting of 150 mM NaCl, 50 mM Tris–HCl pH 7.4, 10 mM NaF, 1 mM Na₃VO₄, 1 mM EDTA, 1% (v/v) Triton X-100, 0.5% (w/v) Na-deoxycholate, 0.1% (w/v) SDS (all from Sigma-Aldrich, St. Louis, MO, USA), and ¼ of a cComplete Mini EDTA-free protease inhibitor tablet (Roche, Basel, Switzerland) in 10 mL buffer. Cells were scraped and the collected lysate was shaken at 4 °C for 5 min at 750 rpm (Thermo-Shaker, Universal Labortechnik GmbH & Co. KG, Leipzig, Germany). Lysate and cell fragments were separated by centrifugation at 4 °C for 20 min at 12,000 rpm (Centrifuge 5418 R, Eppendorf, Hamburg, Germany). Protein concentrations in the supernatant were determined using the Pierce Micro BCA Protein Assay kit (Thermo Fisher Scientific, Waltham, MA, USA) according to the manufacturer's protocol.

SDS-PAGE was performed to analyze the time-dependent phosphorylation of HER2 upon ligand stimulation. Pre-cast 4–20% gradient SDS-PAGE gels (Mini-PROTEAN[®] TGX[™], BioRad Laboratories, Hercules, CA, USA) were mounted in a cask filled with running buffer (25 mM Tris base, 190 mM glycine, 3.5 mM SDS, pH 8.3, all from Sigma-Aldrich). 50 μg protein was prepared in 20% (v/v) loading dye [250 mM Tris–HCl (pH 6.8), 8% (w/v) SDS, 0.1% (w/v) bromophenol blue (all from Sigma-Aldrich), and 40% (v/v) glycerol (Carl Roth, Karlsruhe, Germany)], supplied with 0.1 M dithiothreitol (Sigma-Aldrich), heated to 95 °C for 5 min and loaded onto the gel with PageRuler[™] Prestained Protein Ladder (Thermo Fisher Scientific) as a reference marker. Gels were run at 60 V for 10 min to allow the samples to enter the gel and then at 200 V for 45 min.

Gels were blotted for 7 min using an iBlot Gel Transfer Device (Invitrogen). All further incubation steps were performed under agitation at room temperature if not stated otherwise. First, blots were incubated in blocking buffer [5% (w/v) milk powder (nonfat dry milk, Cell Signaling Technology, Danvers, MA, USA)] in TBST containing 25 mM

Tris base, 150 mM NaCl, and 0.05% (v/v) Tween-20 (all from Sigma-Aldrich) in water, pH 7.6, for 1 h. After washing three times with TBST for 5 min, the blots were incubated with primary antibodies against HER2 (rabbit anti-HER2^{Y1221/1222}, Cell Signaling Technology #2243, diluted 1:500 for EGF-, TGF α -, and EREG-stimulated samples, diluted 1:200 for NRG β 1-stimulated samples) and a house-keeping gene (rabbit anti-actin, abcam #ab14130, diluted 1:40,000 for all conditions) in TBST supplemented with 5% (w/v) BSA (Sigma-Aldrich) at 4 °C overnight. Blots were washed three times with TBST for 5 min prior to the addition of the secondary antibody (goat anti-rabbit tagged with horseradish peroxidase, Jackson ImmunoResearch, West Grove, PA, USA, #111-035-003, diluted 1:20,000) in TBST supplemented with 5% (w/v) BSA (Sigma-Aldrich). The secondary antibody was incubated for 3 h. Afterward, blots were washed four times with TBST for 5 min, 10 min, 15 min, and 15 min, respectively. Lastly, washing with TBS was performed for 5 min. For imaging, blots were treated with SuperSignal West Femto Maximum Sensitivity Substrate (Thermo Fisher Scientific) according to the manufacturer's protocol, and bands were detected on a CHEMI-only chemiluminescence imaging system (VWR, Radnor, PA, USA).

Statistical analysis

Statistical analysis was performed with *OriginPro 2022* (v9.9.0.225, OriginLab Corporation, Northampton, MA, USA). Mean values were calculated for all diffusion properties of individual cells and displayed with their respective standard errors. Populations were tested for being normally distributed using the Shapiro–Wilk test ($\alpha=0.05$). As some populations rejected this hypothesis, non-parametric tests were chosen for comparing data. The Mann–Whitney *U* test was used to compare distributions from different treatment groups, whereas Wilcoxon signed-rank tests were used to validate data from the same treatment group. The following classification of significance levels was used: $p \geq 0.05$ no significant difference (not labeled), $p < 0.05$ significant difference (*), $p < 0.01$ very significant difference (**), $p < 0.001$ highly significant difference (***)

Results

We investigated the activation strength of HER2 in live HeLa cells treated with different ligands that target its heterodimerization partners EGFR, HER3, or HER4. For that purpose, we measured the diffusion coefficient and type of HER2 in unstimulated and ligand-stimulated HeLa cells using single-particle tracking (SPT) [49] with the fluorophore-conjugated nanobody 2Rs15d [55] (Fig. 1A). This

nanobody was found to only bind domain I of the HER2 receptor [11] and to not compete with HER2-specific inhibitors trastuzumab and pertuzumab [55], which target the dimerization interface of the receptor [7, 16, 31]. Hence, this nanobody does not, or only to a small extent, impair the formation of heterodimers of HER2 with EGFR, HER3, and HER4 which occurs through domain II of the HER2 receptor [23]. We were able to confirm this by western blot analysis (Fig. S1).

First, we investigated how ligand activation of EGFR, a heterodimerization partner of HER2 [18, 19], impacts the mobility of HER2 receptors. We selected the ligands EGF and TGF α , which exclusively bind to EGFR [37], and measured the diffusion coefficient of single HER2 receptors in the basal plasma membrane of live HeLa cells. In untreated cells, we found a bimodal distribution of the diffusion coefficients of HER2 (Fig. 1B), from which we calculated a global diffusion coefficient of $D_{\text{global}} = 0.125 \pm 0.005 \mu\text{m}^2/\text{s}$ (Fig. 1C). In cells treated with EGFR-targeting ligands EGF or TGF α , we found a decrease in the fraction of HER2 receptors with high diffusion coefficients, and an increase in the fraction with low diffusion coefficients, with EGF showing a stronger effect than TGF α (Fig. 1B). This was mirrored in a decrease of the global diffusion coefficients, which were calculated to $D_{\text{global,EGF}} = 0.102 \pm 0.005 \mu\text{m}^2/\text{s}$ and $D_{\text{global,TGF}\alpha} = 0.111 \pm 0.005 \mu\text{m}^2/\text{s}$ for cells treated with EGF or TGF α , respectively (Fig. 1C). Next, we analyzed the mode of diffusion [41] and distinguished immobile HER2 receptors from those showing confined or free diffusion (Fig. 1D–F). For HER2 in untreated cells, we found $10.5 \pm 0.4\%$ immobile receptors, whereas $28.1 \pm 0.4\%$ and $61.4 \pm 0.6\%$ showed confined or free diffusion, respectively (Fig. 1E). In cells treated with EGF and TGF α , we observed an increase in the immobile fraction of HER2 receptors, at the expense of freely diffusing receptors. For cells treated with EGF, we determined the fraction of immobile HER2 receptors to 22.7%, which corresponds to an increase of 116%. In cells treated with TGF α , we found a smaller increase in the immobile fraction to 14.9%, which corresponds to an increase of 42%. At the same time, we found that the diffusion coefficient of the fraction of freely or confined diffusing HER2 receptors was reduced in cells treated with EGF or TGF α (Fig. 1F). Changes in the quantity of immobile receptors indicate HER2 activation and ligand-specific responses. The amount of immobile receptors in untreated cells could partly also arise from unspecifically bound nanobody to the cell surface. As a control experiment, we measured the diffusion coefficient and type of a transmembrane domain (TMD) peptide conjugated to mEGFP (mEGFP–TMD) that was targeted with a fluorophore-labeled anti-GFP nanobody [56] and of a GPI conjugated to mEos3.2 [21]. We found no significant difference in the diffusion coefficient of, nor changes in the diffusion type

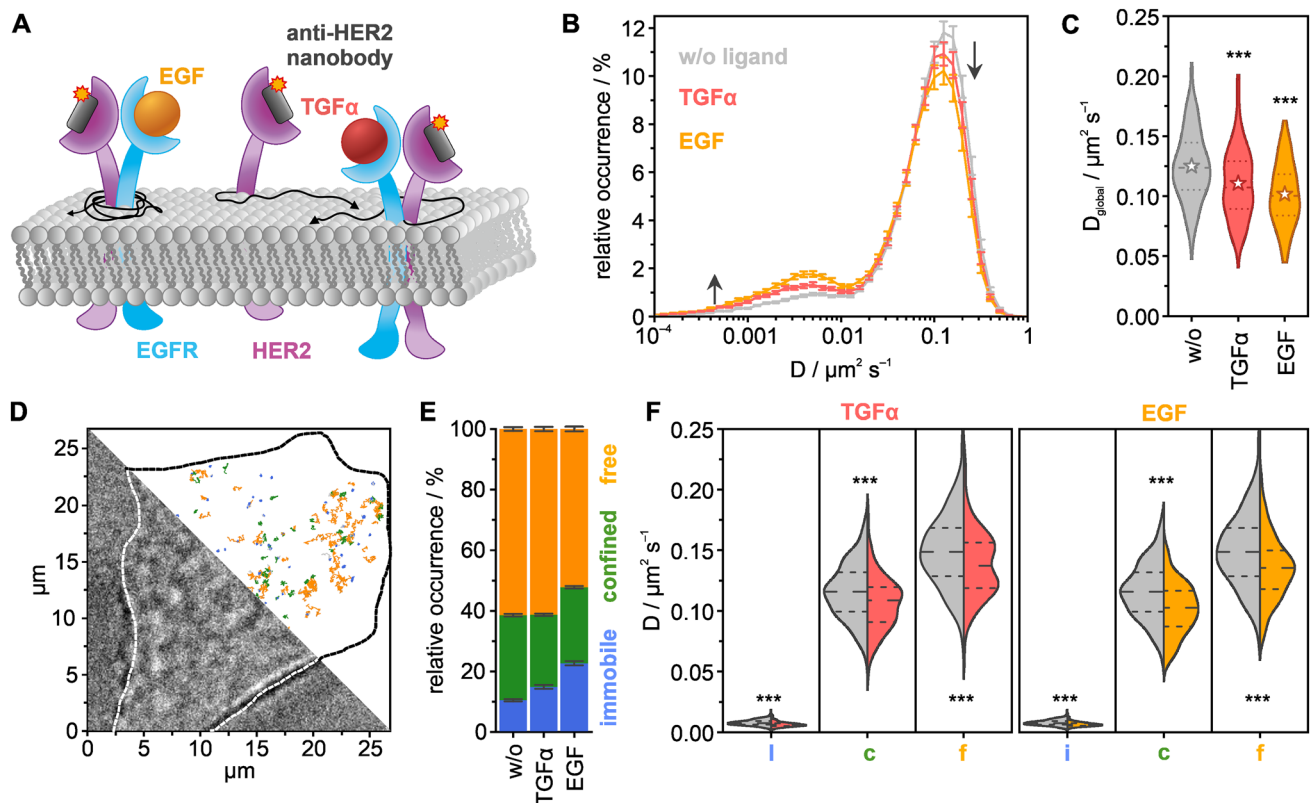


Fig. 1 Single-particle tracking of HER2 in live HeLa cells treated with the EGFR-targeting ligands EGF and TGF α . **A** HER2 was targeted with a Cy3B-labeled anti-HER2 nanobody, and the mobility of HER2 was measured in the absence and presence of EGF and TGF α . **B** Distribution of diffusion coefficients for resting (gray), EGF- (orange), and TGF α -treated (red) HeLa cells at 22 °C. **C** Global diffusion coefficient per condition (violin plots with dotted lines marking the quartiles, dashed lines the median, and stars representing mean values). **D** Exemplary bright-field image of a living HeLa cell treated with EGF, and single-molecule trajectories colored for their diffusion

mode, immobile (blue), confined (green), and free (orange). **E** Relative occurrences of immobile, confined, and freely diffusing HER2 receptors in live HeLa cells. **F** The diffusion coefficient for the individual diffusion modes: immobile (i), confined (c), and free (f) (violin plots, dense dashed lines represent the quartiles, loosely dashed lines represent the median). The data shown was assembled from 160 cells. Error bars are defined by SEMs; $p > 0.05$ no significant difference (no label), $p < 0.05$ significant difference (*), $p < 0.01$ very significant difference (**), $p < 0.001$ highly significant difference (***)

for mEGFP-TMD or GPI-mEos3.2 in untreated and EGF-treated cells (Fig. S2, Tables S1–S8). Furthermore, we monitored key parameters of all SPT experiments in untreated and ligand-treated cells and calculated the average number of trajectories and segments per cell and trajectory as well as segment lengths for all conditions (Fig. S3).

Next, we investigated the activation of HER2 in cells treated with EREG, which predominantly binds HER4 as well as EGFR, and with NRG β 1, which binds to HER3 and HER4 [37], by measuring the mobility of HER2 receptors in live HeLa cells (Fig. 2A). We found that the bimodal distribution of the diffusion coefficients of HER2 showed small changes in cells treated with EREG or NRG β 1, as compared to untreated cells (Fig. 2B). This is reflected in smaller changes of the global diffusion coefficient, $D_{\text{global,EREG}} = 0.113 \pm 0.005 \mu\text{m}^2/\text{s}$ and $D_{\text{global,NRG}\beta 1} = 0.121 \pm 0.005 \mu\text{m}^2/\text{s}$, for EREG and NRG β 1, respectively (Fig. 2C). The analysis of diffusion types of

single trajectories (Fig. 2D) showed that the fraction of immobile receptors increased from $10.5 \pm 0.4\%$ in untreated cells to $12.5 \pm 0.5\%$ and $16.5 \pm 0.5\%$ in cells treated with NRG β 1 or EREG, respectively, and at the expense of a decrease of the mobile fraction (Fig. 2E). Again, we found that the diffusion coefficient of the fraction of freely or confined diffusing HER2 receptors was reduced in cells treated with EREG or NRG β 1 (Fig. 2F).

The experiments were further refined to follow the activation of HER2 receptors in live cells over longer time periods, using the diffusion coefficient and type as proxies for the formation of heterodimers with EGFR, HER3, or HER4. Since the observation time of HER2 receptors bound to a fluorophore-labeled nanobody is limited by photobleaching, the time window for the observation of a single cell is too short to follow changes related to signaling activation that typically occur at the time scale of minutes [26]. To bypass this limitation, we established an experimental procedure in

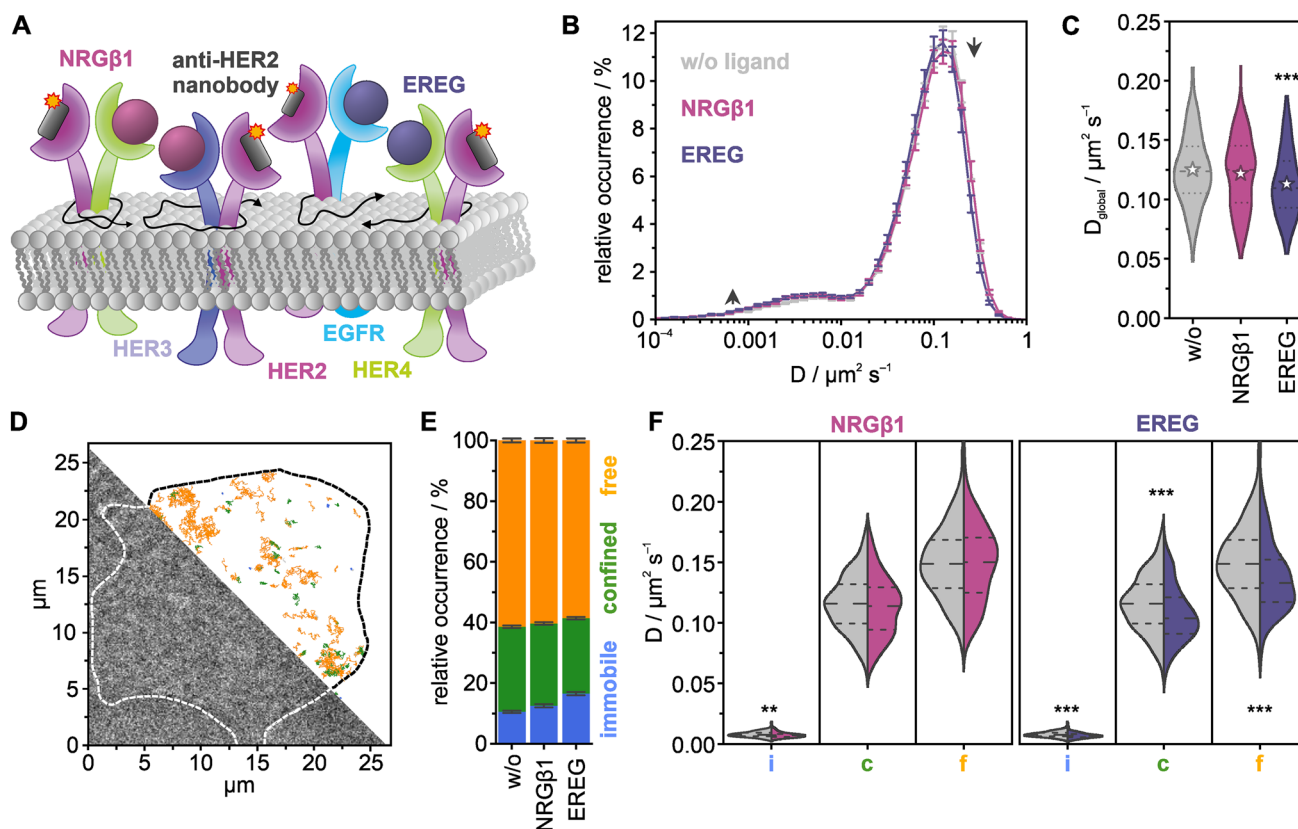


Fig. 2 Single-particle tracking of HER2 in live HeLa cells treated with the ligands EREG and NRG β 1. **A** HER2 was targeted with a Cy3B-labeled anti-HER2 nanobody, and the mobility of HER2 was measured in the absence and presence of EREG and NRG β 1. **B** Distribution of diffusion coefficients for resting (gray), EREG- (purple), and NRG β 1-treated (lilac) HeLa cells at 22 °C. **C** Global diffusion coefficient per condition (violin plots with dotted lines marking the quartiles, dashed lines the median, and stars representing mean values). **D** Exemplary bright-field image of a living HeLa cell treated with NRG β 1, and single-molecule trajectories colored for their diffu-

sion mode, immobile (blue), confined (green), free (orange). **E** Relative occurrences of immobile, confined, and freely diffusing HER2 receptors in live HeLa cells. **F** The diffusion coefficient for the individual diffusion modes immobile (i), confined (c), and free (f) (violin plots, dense dashed lines represent the quartiles, loosely dashed lines represent the median). The data shown was assembled from 160 cells. Error bars are defined by SEMs; $p > 0.05$ no significant difference (no label), $p < 0.05$ significant difference (*), $p < 0.01$ very significant difference (**), $p < 0.001$ highly significant difference (***)

which we measured many cells sequentially, giving each cell its own time stamp (see “Materials and methods”) (Fig. 3A). Using that procedure, we measured the diffusion coefficient and type of single HER2 receptors over a period of 25 min in the same well. The respective ligand was added after 5 min, to record reference data for untreated cells; this enabled it to follow ligand-specific changes in diffusion coefficient and type for a time of 20 min.

We analyzed the diffusion type and coefficient over time for all four ligands, EGF, TGF α , EREG, and NRG β 1 (Fig. 3B, C; S4–S7). Considering our previous result of an increase in the immobile fraction of HER2 in ligand-treated cells (Figs. 1E, 2E), we followed the population of the immobile fraction over time (Figs. 3B; S6C). For all ligands, we found a strong increase of the immobile fraction after 5 min, which represented at the same time the maximum in cells treated with the ligands EGF, TGF α , and

EREG. In cells treated with NRG β 1, we found the maximum population of the immobile fraction shifted to ~10 min. In cells treated with EGF, the fraction of immobile HER2 increased by 180% after 5 min of stimulation before slowly decreasing to ~60% within the following 15 min (Fig. 3Bi). In cells treated with TGF α and EREG, the fraction of immobile particles increased to a maximum of ~120% and 100%, respectively, compared to unstimulated cells (Figs. 3Bii, iii), while changes observed for cells treated with NRG β 1 were smaller (Fig. 3Biv). While the population of immobile particles returned to the level found in untreated cells for TGF α , EREG, and NRG β 1, this was not found for EGF. To correlate the increase in the population of the immobile state with the activation of HER2, we performed a western blot analysis of phosphorylated HER2 for all four ligands at different time points (Fig. 3B; S8). We found the maximum population of phosphorylated HER2 around 2–5 min

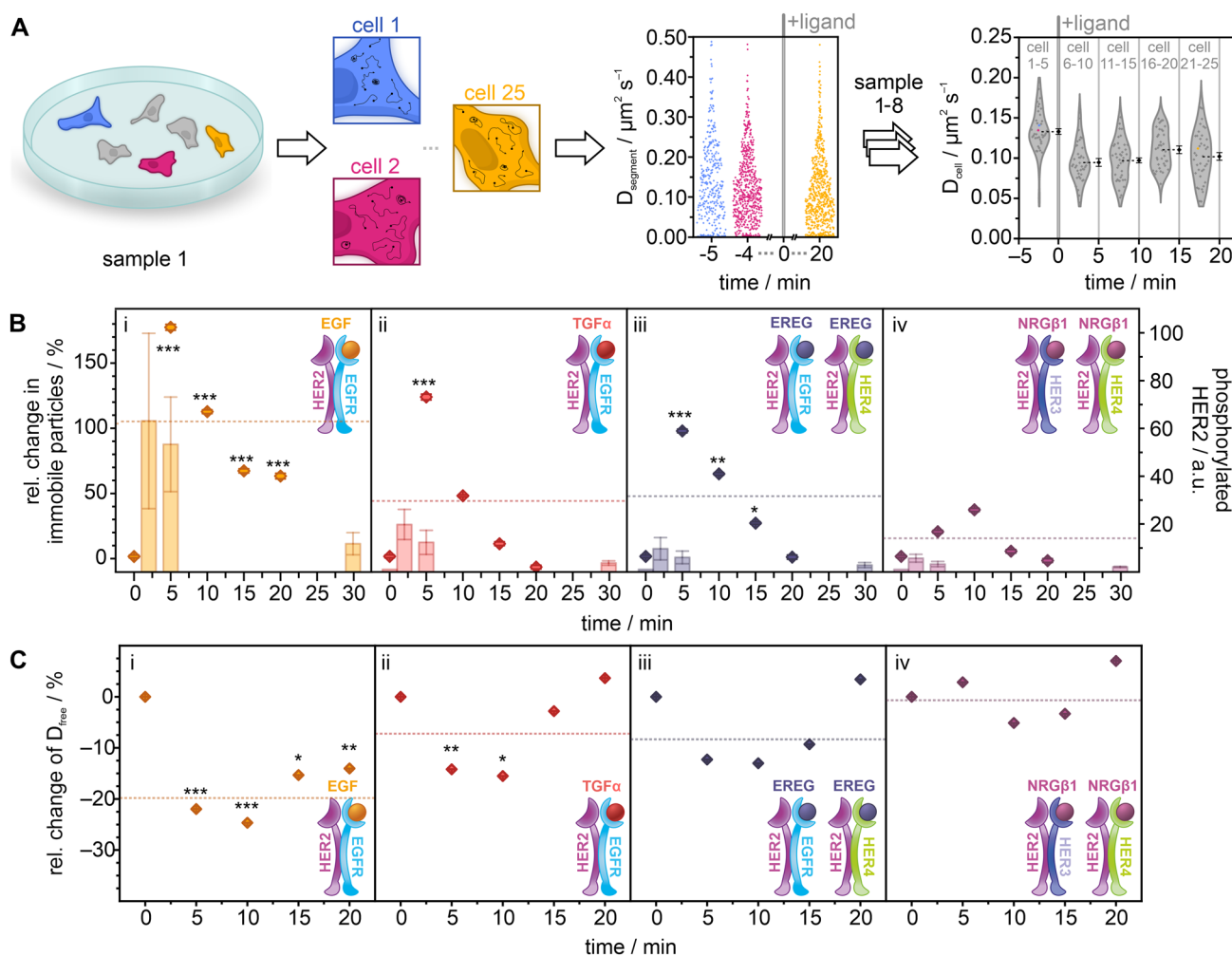


Fig. 3 Temporal response of HER2 activation in living HeLa cells following treatment with EGF, TGF α , EREG, or NRG β 1. **A** Schematic representation of the time-course SPT experiment. Cells were seeded sparsely and imaged sequentially. After imaging 5 cells in resting condition, the respective ligand was added to the cell dish and the measurement continued. Diffusion mode and coefficients were calculated per cell and pooled into 5 min time intervals. Diamonds represent mean diffusion coefficients per segment (colored) or cell (grey; mean values are colored in black with error bars representing the SEM). **B** Relative change in the fraction of immobile particles (dot plots) plotted against time. Bars show HER2 phosphorylation obtained from western blots ($N=3$). **C** Relative change in the

diffusion coefficient of freely diffusing particles over time. Relative changes were calculated from mean values of 40 cells per interval. Receptor models indicate the expected ligand-orchestrated interactions between HER2 and other receptors of the family. The dotted lines represent mean values of the relative change over the time of ligand stimulation. Error bars in dot plots represent the standard error of the difference (SED); error bars in bar plots show the standard error of the mean (SEM). Significance was tested for stimulated cells vs. untreated cells from the same sample before calculating the relative change; $p > 0.05$ no significant difference (no label), $p < 0.05$ significant difference (*), $p < 0.01$ very significant difference (**), $p < 0.001$ highly significant difference (***)

for all four ligands, similar to the population maxima of the immobile state. The activation strengths for phosphorylated HER2 were strongest for EGF, followed by TGF α and EREG (Fig. 3B; S8).

The population of the fractions of freely and confined diffusing HER2 also showed a first response after 5 min, with different temporal signatures and strengths for the different ligands (Figs. S4; S6A, B). For all four ligands, we measured a reduced diffusion coefficient for the freely diffusing population of HER2, amounting to ~5% (NRG β 1), ~15% (TGF α ,

EREG), and ~25% (EGF) (Figs. 3C; S7A). We further found that this change was shifted to later time points of ~10 min for all receptors. For cells treated with TGF α , EREG, or NRG β 1, we found that after 20 min, the diffusion coefficient showed similar values as in untreated cells, whereas this was not the case for cells treated with EGF. The diffusion coefficient of confined HER2 receptors shows a similar temporal signature and strength (Figs. S5A; S7B), while smaller effects were found for the diffusion coefficient of immobile HER2 (Figs. S5B; S7C).

Discussion

Using live-cell single-particle tracking and data analysis, we extracted the diffusion coefficients and modes of HER2 in the native plasma membrane of living HeLa cells. We found that HER2 molecules in the plasma membrane of unstimulated cells exhibit heterogeneity in mobility, including free and confined diffusing as well as immobile receptors. To attribute these states to their potential activity, we first monitored how the population of the mobility states changes upon ligand treatment of known heterodimerization partners of HER2. For all four ligands investigated, EGF, TGF α , EREG, and NRG β 1, we found a decrease in free diffusing HER2 and an increase in immobile HER2. This indicates that free diffusing HER2 promotes encounters with the interaction partners EGFR, HER3, and HER4 and that the heterodimers enrich into immobile receptor complexes. A similar observation was reported for EGFR, which populates a slow diffusion state upon binding EGF [8]. To further support this interpretation for HER2, we performed western blotting and found an increase in phosphorylated HER2 that correlated with the increase of immobile particles. We also found that the global diffusion coefficient of HER2 derived from all HER2 molecules without grouping into diffusion modes was reduced in cells treated with EGF, TGF α , or EREG, with the response being strongest for EGF. This reduction was also reflected in the diffusion coefficient for free and confined diffusing HER2 molecules in cells treated with EGF, TGF α , or EREG.

Our single-molecule imaging method allowed following the movement of single HER2 molecules for up to a few seconds, limited by photobleaching. Signaling initiation of ErbB receptors, however, occurs at the time scale of minutes [22]. An elegant strategy to bridge these two time windows is to measure the mobility of single receptors in many different cells of the same dish sequentially, as it was reported for VEGFR-2 recently and allowed to follow receptor activation after ligand stimulation [44]. We adapted this concept and established a time-course single-particle experiment by measuring HER2 mobility in many cells from the same dish sequentially. We measured the activation of HER2 in response to different ligands that target its heterodimerization partners for up to 30 min. Each measured cell was time stamped, resulting in a temporal profile of HER2 mobility following ligand treatment of cells. This information-rich data informed on the temporal signature of HER2 activation, its strength, and desensitization over time, for the respective ligand. Commonly for all four ligands investigated, we found an enrichment in immobile HER2 molecules peaking at 5–10 min after ligand treatment, paralleled by a

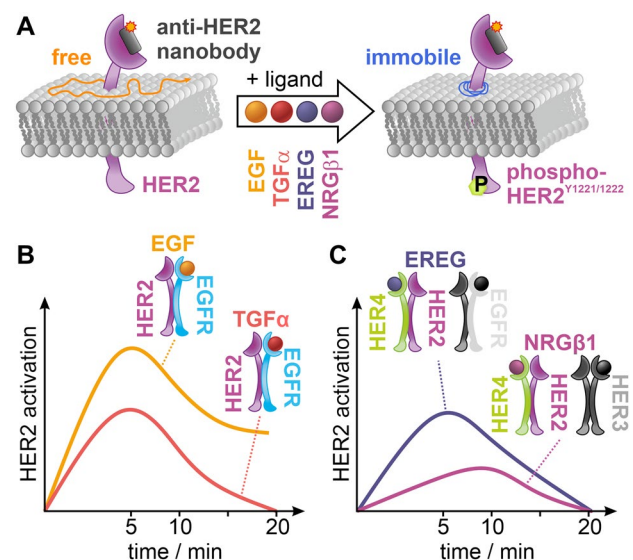


Fig. 4 Proposed model for ligand-induced activation of HER2 derived from single-particle tracking data shown in a model-like fashion by means of the active population. **A** In cells treated with EGF, TGF α , EREG, or NRG β 1, the population of immobile HER2 increases at the cost of freely diffusing HER2. This increase scales with the formation of phosphorylated HER2. **B** Temporal profile, strength, and decay of HER2 activation in cells treated with the EGFR-targeting ligands EGF and TGF α . **C** Temporal profile, strength, and decay of HER2 activation in cells treated with the ligand EREG and NRG β 1

decrease of freely diffusing HER2 molecules. The strength of HER2 activation, measured as the increase of enrichment of immobile particles and supported by western blot data of HER2 phosphorylation (Fig. 4A), was highest for EGF, followed by TGF α and EREG, and the weakest for NRG β 1. The diffusion coefficient of mobile HER2 molecules decreased for all ligands by 10–25%, with the extent of decrease being highest for EGF, followed by TGF α , EREG, and NRG β 1. These ligand-induced changes in diffusion mode and coefficient are very similar to recently reported results for the receptor tyrosine kinase VEGFR-2 [44]. The temporal profile of HER2 activation by EGF is also in line with a reported systems biology model [22].

EGF and TGF α bind exclusively to EGFR and with similar affinity [30, 34, 48], yet initiate differential intracellular signaling responses [1, 13, 27, 28, 48, 57, 58]. Both ligands were reported to exhibit an increased affinity for EGFR/HER2 heterodimers compared with EGFR homodimers [32]. The temporal profiles of HER2 activation, derived from an increase in immobile HER2 molecules and the parallel decrease of free HER2 molecules, peak at 5 min for both EGF and TGF α , but differ in strength, with EGF superseding TGF α (Fig. 4B). The desensitization of TGF α is complete after 20 min, when both the immobile and freely diffusing HER2 molecules return to levels in unstimulated cells, yet not for EGF, where about

40% of HER2 molecules remain immobile after 20 min. These results suggest that HER2 is preferably recruited to EGF-bound EGFR, which agrees with biochemical data reporting that TGF α has a reduced ability to recruit EGFR into heterodimers with HER2 [19]. The results also show that the different signaling responses initiated by EGF and TGF α are mirrored in the temporal profile of diffusion mode population and diffusion coefficient.

REG and NRG β 1 both bind to HER4, with REG showing weak affinity to EGFR, and NRG β 1 also binding to HER3 [25, 43]. The temporal profiles of HER2 activation, derived from an increase in immobile HER2 molecules and the parallel decrease of free HER2 molecules, showed a peak at 5 min for REG and at 10 min for NRG β 1 (Fig. 4C). In addition, we found a strong activation of HER2 by REG and a rather weak activation by NRG β 1. NRG β 1 is reported to strongly bind both HER3 and HER4 [25]. However, the expression level of HER3 in HeLa cells is lower than that of HER4 (Fig. S9), and HER3 is reported to mainly localize intracellularly [6] (Supplemental Note 2), suggesting that the observed activation of HER2 in response to NRG β 1 can be mainly attributed to HER2/HER4 heterodimer formation. REG is a low-affinity ligand to EGFR [17] while binding HER4 with high affinity [25]. This suggests that the observed activation of HER2 in response to REG can be mainly ascribed to HER2/HER4 heterodimer formation. In consequence, the activation strength of HER2 through the formation of HER2/HER4 heterodimers is stronger for REG than for NRG β 1, indicating a bias in signaling activation.

In summary, we found activation patterns for HER2 in live cells that differed for the four ligands investigated. EGF and TGF α , both binding EGFR, show a stronger activation of HER2 than REG and NRG β 1, predominantly binding to HER4 in HeLa cells (Supplemental Note 2). In part, this might be related to differences in the protein expression level of EGFR and HER4 (Fig. S9B), which to some degree influences the probability of receptor encounter and heterodimer formation. For both pairs of ligands that lead to the formation of the respective heterodimers EGFR/HER2 (binding of EGF or TGF α to EGFR) and HER4/HER2 (binding of REG or NRG β 1 to HER4), we found a different activation strength of HER2. Since these ligands also initiate differential intracellular signaling responses for their target receptors EGFR [1, 13, 27, 28, 48, 57, 58] and HER4 [25], this indicates that HER2 heterodimers with EGFR and HER4 show a selective response to the respective ligand or biased signaling.

Conclusion

We measured the plasma membrane mobility of HER2 in live HeLa cells treated with various ligands targeting the heterodimerization partners EGFR, HER3, and HER4. We extracted diffusion coefficient and type, monitored specific

changes in ligand-treated cells, and found different activation strengths for the heteromeric receptor complexes with EGFR and HER4. By measuring the diffusion properties of single HER2 receptors in many single cells sequentially, we were able to monitor how the diffusion states of HER2 change over longer time periods. The temporal profile of diffusion states hereby correlated well to the reported kinetics of signaling activation through HER2, indicating that diffusion properties can serve as proxies to follow the activation of HER2 in heteromeric receptor complexes. This allowed us to characterize ligand-specific activation profiles related to the formation of the different heteromeric receptor complexes, for which we found distinguishable activation kinetics, activation strength, and diffusion fingerprints. This contributes to our understanding of the biased activation of HER2 heterodimers, and the approach is transferable to other membrane receptors targeted by multiple ligands.

Supplementary Information The online version contains supplementary material available at <https://doi.org/10.1007/s00018-023-04806-8>.

Acknowledgements We are grateful to Prof. Jacob Piehler for generously providing the plasmid for mEGFP-TMD and for helpful discussions. We thank Petra Freund for assistance in cell culture and Yunqing Li and Sinem Bulmus for helpful discussions.

Author contributions MH designed the research. LT, MO, and JK produced and labeled the nanobody. CC performed live-cell single-molecule imaging experiments with support from MSD. JVR programmed the analysis software. CC performed image analysis with support from JVR and MSD. CC, MSD, and MH wrote the manuscript with contributions from all authors.

Funding Open Access funding enabled and organized by Projekt DEAL. We gratefully acknowledge the Deutsche Forschungsgemeinschaft (Grants CRC1507 and RTG2556) and LOEWE (FCI) for financial support. This work was supported by the Danish National Research Foundation (CellPAT; DNRF135) and by the Novo Nordisk foundation (CEMBID; NNF17OC0028070).

Data availability The datasets generated during the current study are available in the EMBL BioImaging Archive, <https://www.ebi.ac.uk/biostudies/bioimages/studies/S-BIAD597>.

Declarations

Conflict of interest The authors declare no competing interests.

Open Access This article is licensed under a Creative Commons Attribution 4.0 International License, which permits use, sharing, adaptation, distribution and reproduction in any medium or format, as long as you give appropriate credit to the original author(s) and the source, provide a link to the Creative Commons licence, and indicate if changes were made. The images or other third party material in this article are included in the article's Creative Commons licence, unless indicated otherwise in a credit line to the material. If material is not included in the article's Creative Commons licence and your intended use is not permitted by statutory regulation or exceeds the permitted use, you will need to obtain permission directly from the copyright holder. To view a copy of this licence, visit <http://creativecommons.org/licenses/by/4.0/>.


References

1. Barranton Y, Green H (1987) Cell migration is essential for sustained growth of keratinocyte colonies: the roles of transforming growth factor- α and epidermal growth factor. *Cell* 50(7):1131–1137
2. Carpenter G, Lembach KJ, Morrison MM, Cohen S (1975) Characterization of the binding of ¹²⁵I-labeled epidermal growth factor to human fibroblasts. *J Biol Chem* 250(11):4297–4304
3. Casaletto JB, McClatchey AI (2012) Spatial regulation of receptor tyrosine kinases in development and cancer. *Nat Rev Cancer* 12(6):387–400
4. Casalini P, Iorio MV, Galmozzi E, Ménard S (2004) Role of HER receptors family in development and differentiation. *J Cell Physiol* 200(3):343–350
5. Chan SD, Antonucci DM, Fok KS, Alajoki ML, Harkins RN, Thompson SA, Wada HG (1995) Heregulin activation of extracellular acidification in mammary carcinoma cells is associated with expression of HER2 and HER3. *J Biol Chem* 270(38):22608–22613
6. Chen B, Mao R, Wang H, She J (2010) Cell line and drug-dependent effect of ERBB3 on cancer cell proliferation, chemosensitivity, and multidrug actions. In: *International journal of high throughput screening*, April, 49
7. Cho H-S, Mason K, Ramyar KX, Stanley AM, Gabelli SB, Denney Jr DW, Leahy DJ (2003) Structure of the extracellular region of HER2 alone and in complex with the herceptin fab. *Nature* 421(6924):756–760
8. Chung I, Akita R, Vandlen R, Toomre D, Schlessinger J, Mellman I (2010) Spatial control of EGF receptor activation by reversible dimerization on living cells. *Nature* 464(7289):783–787
9. Coussens L, Yang-Feng TL, Liao YC, Chen E, Gray A, McGrath J, Seeburg PH, Libermann TA, Schlessinger J, Francke U (1985) Tyrosine kinase receptor with extensive homology to EGF receptor shares chromosomal location with Neu oncogene. *Science* 230(4730):1132–1139
10. de Bono JS, Rowinsky EK (2002) The ErbB receptor family: a therapeutic target for cancer. *Trends Mol Med* 8(4 Suppl):S19–26
11. D'Huyvetter M, De Vos J, Xavier C, Pruszynski M, Sterckx YGJ, Massa S, Raes G et al (2017) ¹³¹I-labeled anti-HER2 camelid sdAb as a theranostic tool in cancer treatment. *Clin Cancer Res* 23(21):6616–6628
12. Du Z, Lovly CM (2018) Mechanisms of receptor tyrosine kinase activation in cancer. *Mol Cancer* 17(1):58
13. Ebner R, Derynck R (1991) Epidermal growth factor and transforming growth factor- α : differential intracellular routing and processing of ligand-receptor complexes. *Cell Regul* 2(8):599–612
14. Edelstein AD, Tsuchida MA, Amodaj N, Pinkard H, Vale RD, Sturman N (2014) Advanced methods of microscope control using μ Manager software. *J Biol Methods*. <https://doi.org/10.1444/jbm.2014.36>
15. Fraguas S, Barberán S, Cebrià F (2011) EGFR signaling regulates cell proliferation, differentiation and morphogenesis during planarian regeneration and homeostasis. *Dev Biol* 354(1):87–101
16. Franklin MC, Carey KD, Vajdos FF, Leahy DJ, de Vos AM, Sliwkowski MX (2004) Insights into ErbB signaling from the structure of the ErbB2-pertuzumab complex. *Cancer Cell* 5(4):317–328
17. Freed DM, Bessman NJ, Kiyatkin A, Salazar-Cavazos E, Byrne PO, Moore JO, Valley CC et al (2017) EGFR ligands differentially stabilize receptor dimers to specify signaling kinetics. *Cell* 171(3):683–95.e18
18. Graus-Porta D, Beerli RR, Daly JM, Hynes NE (1997) ErbB-2, the preferred heterodimerization partner of all ErbB receptors, is a mediator of lateral signaling. *EMBO J* 16(7):1647–1655
19. Gulliford TJ, Huang GC, Ouyang X, Epstein RJ (1997) Reduced ability of transforming growth factor- α to induce EGF receptor heterodimerization and downregulation suggests a mechanism of oncogenic synergy with ErbB2. *Oncogene* 15(18):2219–2223
20. Harwardt M-L, Young P, Bley Müller WM, Meyer T, Karathanasis C, Niemann HH, Heilemann M, Dietz MS (2017) Membrane dynamics of resting and internalin B-bound MET receptor tyrosine kinase studied by single-molecule tracking. *FEBS Open Bio* 7(9):1422–1440
21. Harwardt M-L, Dietz M, Heilemann M, Wohland T (2018) SPT and imaging FCS provide complementary information on the dynamics of plasma membrane molecules. *Biophys J* 114(10):2432–2443
22. Hass H, Masson K, Wohlgemuth S, Paragas V, Allen JE, Sevecka M, Pace E et al (2017) Predicting ligand-dependent tumors from multi-dimensional signaling features. *NPJ Syst Biol Appl* 3(September):27
23. Hu S, Sun Y, Meng Y, Wang X, Yang W, Wenyan Fu, Guo H et al (2015) Molecular architecture of the ErbB2 extracellular domain homodimer. *Oncotarget* 6(3):1695–1706
24. Ibach J, Radon Y, Gelléri M, Sonntag MH, Brunsveld L, Bastiaens PIH, Vermeer PJ (2015) Single particle tracking reveals that EGFR signaling activity is amplified in clathrin-coated pits. *PLoS ONE* 10(11):e0143162
25. Jones JT, Akita RW, Sliwkowski MX (1999) Binding specificities and affinities of EGF domains for ErbB receptors. *FEBS Lett* 447(2–3):227–231
26. Kiso-Farnè K, Tsuruyama T (2022) Epidermal growth factor receptor cascade prioritizes the maximization of signal transduction. *Sci Rep* 12(1):16950
27. Knudsen SL, Jeppe AS, Mac W, Henriksen L, van Deurs Bo, Grøvdal LM (2014) EGFR signaling patterns are regulated by its different ligands. *Growth Fact* 32(5):155–163
28. Korc M, Haussler CA, Trookman NS (1987) Divergent effects of epidermal growth factor and transforming growth factors on a human endometrial carcinoma cell line. *Can Res* 47(18):4909–4914
29. Kraus MH, Issing W, Miki T, Popescu NC, Aaronson SA (1989) Isolation and characterization of ERBB3, a third member of the ERBB/epidermal growth factor receptor family: evidence for overexpression in a subset of human mammary tumors. *Proc Natl Acad Sci USA* 86(23):9193–9197
30. Lax I, Johnson A, Howk R, Sap J, Bellot F, Winkler M, Ullrich A, Vennstrom B, Schlessinger J, Givol D (1988) Chicken epidermal growth factor (EGF) receptor: cDNA cloning, expression in mouse cells, and differential binding of EGF and transforming growth factor α . *Mol Cell Biol* 8(5):1970–1978
31. Leahy DJ (2004) Structure and function of the epidermal growth factor (EGF/ErbB) family of receptors. *Adv Protein Chem* 68:1–27
32. Macdonald-Obermann JL, Pike LJ (2014) Different epidermal growth factor (EGF) receptor ligands show distinct kinetics and biased or partial agonism for homodimer and heterodimer formation. *J Biol Chem* 289(38):26178–26188
33. Martínez-Mañoz L, Rodríguez-Frade JM, Barroso R, Carlos ÓS, Sorzano JA, Torreño-Pina CA, Santiago CM et al (2018) Separating actin-dependent chemokine receptor nanoclustering from dimerization indicates a role for clustering in CXCR4 signaling and function. *Mol Cell* 70(1):106–19.e10
34. Massagué J (1983) Epidermal growth factor-like transforming growth factor. II. Interaction with epidermal growth factor receptors in human placenta membranes and A431 cells. *J Biol Chem* 258(22):13614–13620
35. Michalet X (2010) Mean square displacement analysis of single-particle trajectories with localization error: Brownian motion in

- an isotropic medium. *Phys Rev E Stat Nonlinear Soft Matter Phys* 82(41):041914
36. Momboisse F, Nardi G, Colin P, Hery M, Cordeiro N, Blachier S, Schwartz O et al (2022) Tracking receptor motions at the plasma membrane reveals distinct effects of ligands on CCR5 dynamics depending on its dimerization status. *Elife*. <https://doi.org/10.7554/eLife.76281>
 37. Olaiyoye MA, Neve RM, Lane HA, Hynes NE (2000) The ErbB signaling network: receptor heterodimerization in development and cancer. *EMBO J* 19(13):3159–3167
 38. Ovesný M, Křížek P, Borkovec J, Svindrych Z, Hagen GM (2014) ThunderSTORM: a comprehensive ImageJ Plug-in for PALM and STORM data analysis and super-resolution imaging. *Bioinformatics* 30(16):2389–2390
 39. Park SK, Miller R, Krane I, Vartanian T (2001) The erbB2 gene is required for the development of terminally differentiated spinal cord oligodendrocytes. *J Cell Biol* 154(6):1245–1258
 40. Plowman GD, Culouscou JM, Whitney GS, Green JM, Carlton GW, Foy L, Neubauer MG, Shoyab M (1993) Ligand-specific activation of HER4/p180erbB4, a fourth member of the epidermal growth factor receptor family. *Proc Natl Acad Sci USA* 90(5):1746–1750
 41. Rahm JV, Malkusch S, Endesfelder U, Dietz MS, Heilemann M (2021) Diffusion state transitions in single-particle trajectories of MET receptor tyrosine kinase measured in live cells. *Front Comput Sci*. <https://doi.org/10.3389/fcomp.2021.757653>
 42. Rahm J, Malkusch S, Endesfelder U, Dietz MS, Heilemann M (2022) Extraction of diffusion state transitions in single-particle tracking data of membrane receptors. In: Gregor I, Erdmann R, Koberlibg F (eds) *Single molecule spectroscopy and superresolution imaging XV*. SPIE. <https://doi.org/10.1117/12.2609681>
 43. Riese DJ 2nd, Cullum RL (2014) Epipegulin: roles in normal physiology and cancer. *Semin Cell Dev Biol* 28(April):49–56
 44. da Rocha-Azevedo B, Lee S, Dasgupta A, Vega AR, de Oliveira LR, Kim T, Kittisopikul M, Malik ZA, Jaqaman K (2020) Heterogeneity in VEGF receptor-2 mobility and organization on the endothelial cell surface leads to diverse models of activation by VEGF. *Cell Rep* 32(13):108187
 45. Rossier O, Octeau V, Sibarita J-B, Leduc C, Tessier B, Nair D, Gatterdam V et al (2012) Integrins $\beta 1$ and $\beta 3$ exhibit distinct dynamic nanoscale organizations inside focal adhesions. *Nat Cell Biol* 14(10):1057–1067
 46. Schindelin J, Arganda-Carreras I, Frise E, Kaynig V, Longair M, Pietzsch T, Preibisch S et al (2012) Fiji: an open-source platform for biological-image analysis. *Nat Methods* 9(7):676–682
 47. Schlessinger J (2000) Cell signaling by receptor tyrosine kinases. *Cell* 103(2):211–225
 48. Schreiber AB, Winkler ME, Derynck R (1986) Transforming growth factor-alpha: a more potent angiogenic mediator than epidermal growth factor. *Science* 232(4755):1250–1253
 49. Shen H, Tauzin LJ, Baiyasi R, Wang W, Moringo N, Shuang Bo, Landes CF (2017) Single particle tracking: from theory to biophysical applications. *Chem Rev* 117(11):7331–7376
 50. Stern DF (2000) Tyrosine kinase signalling in breast cancer: ErbB family receptor tyrosine kinases. *BCR* 2(3):176–183
 51. Sweeney C, Carraway KL 3rd (2000) Ligand discrimination by ErbB receptors: differential signaling through differential phosphorylation site usage. *Oncogene* 19(49):5568–5573
 52. Teodori L, Omer M, Märcher A, Skaanning MK, Andersen VL, Nielsen JS, Oldenburg E, Lin Y, Gothelf KV, Kjems J (2022) Site-specific nanobody-oligonucleotide conjugation for super-resolution imaging. *J Biol Methods* 9(1):e159
 53. Trenker R, Jura N (2020) Receptor tyrosine kinase activation: from the ligand perspective. *Curr Opin Cell Biol* 63(April):174–185
 54. Ullrich A, Schlessinger J (1990) Signal transduction by receptors with tyrosine kinase activity. *Cell* 61(2):203–212
 55. Vaneycken I, Devoogdt N, Van Gassen N, Vincke C, Xavier C, Wernery U, Muyltermans S, Lahoutte T, Caveliers V (2011) Pre-clinical screening of anti-HER2 nanobodies for molecular imaging of breast cancer. *FASEB J* 25(7):2433–2446
 56. Wilmes S, Hafer M, Vuorio J, Tucker JA, Winkelmann H, Löchte S, Stanly TA et al (2020) Mechanism of homodimeric cytokine receptor activation and dysregulation by oncogenic mutations. *Science* 367(6478):643–652
 57. Wilson KJ, Gilmore JL, Foley J, Lemmon MA, Riese DJ 2nd (2009) Functional selectivity of EGF family peptide growth factors: implications for cancer. *Pharmacol Ther* 122(1):1–8
 58. Wilson KJ, Mill C, Lambert S, Buchman J, Wilson TR, Hernandez-Gordillo V, Gallo RM, Ades LMC, Settleman J, Riese DJ 2nd (2012) EGFR ligands exhibit functional differences in models of paracrine and autocrine signaling. *Growth Fact* 30(2):107–116

Publisher's Note Springer Nature remains neutral with regard to jurisdictional claims in published maps and institutional affiliations.

Authors and Affiliations

Claudia Catapano¹ · Johanna V. Rahm¹ · Marjan Omer^{2,3} · Laura Teodori^{2,3} · Jørgen Kjems^{2,3} · Marina S. Dietz¹ · Mike Heilemann¹ 

✉ Mike Heilemann
heilemann@chemie.uni-frankfurt.de

¹ Institute of Physical and Theoretical Chemistry, Goethe-University Frankfurt, Max-Von-Laue-Str. 7, 60438 Frankfurt, Germany

² Interdisciplinary Nanoscience Center (iNANO), Aarhus University, Gustav Wieds Vej 14, 8000 Aarhus C, Denmark

³ Center for Cellular Signal Patterns (CellPAT), Aarhus University, Gustav Wieds Vej 14, 8000 Aarhus C, Denmark